IEEE Access
Multidisciplinary | Rapid Review | Open Access Journal

Received November 11, 2019, accepted December 6, 2019, date of publication December 13, 2019,
date of current version December 31, 2019.

Digital Object Identifier 10.1109/ACCESS.2019.2958944

Research on IPMSM Drive System Control Technology for Electric Vehicle Energy Consumption

LIFU LI AND QIN LIU
School of Mechanical and Automotive Engineering, South China University of Technology, Guangzhou 510641, China
Corresponding author: Qin Liu (liuqin_16@126.com)

This work was supported in part by the Special Fund for Key Area Research and Development Program of Guangdong under Grant 2019B090911002, and in part by the Special Fund for Public Welfare Research and Capacity Construction of Guangdong under Grant 2014B010106004.

ABSTRACT At present, most of the existing control strategies of motor drive system are based on the motor itself, without considering the electric vehicle energy consumption from the perspective of the whole vehicle. Hence, a motor drive system control strategy for electric vehicle energy consumption is proposed in this paper. Combining the electric vehicle driving state with the control of interior permanent magnet synchronous motor (IPMSM), the maximum torque per ampere (MTPA) control strategy of electric vehicle IPMSM based on optimization acceleration curve is established. Then, the proposed method is verified by both Matlab/Simulink simulation and experiment. The simulation and experimental results show that compared with the NEDC urban conditions, the driving range of the electric vehicle drive system control strategy based on optimization acceleration curve has been improved a lot, and the energy consumption per kilometer has also been reduced, which verifies the feasibility and effectiveness of the proposed control strategy.

INDEX TERMS Motor drive system control strategy, electric vehicle, energy consumption, interior permanent magnet synchronous motor (IPMSM), maximum torque per ampere (MTPA), acceleration curve.

I. INTRODUCTION

Up to now, many experts and scholars have carried out research on the drive control system of electric vehicles [1]–[4]. And Owing to the advantages of high efficiency, high power density, high torque, low noise, the interior permanent magnet synchronous motors (IPMSMs) have been widely used in electric vehicle drive control system [5], [6]. Due to the asymmetrical structure of the rotor magnetic circuit and unequal *dq*-axis inductances, the IPMSM will generate reluctance torque during operation. Therefore, the output torque of the IPMSM includes permanent magnet torque and reluctance torque. For the same given torque, there are countless distribution modes of the *dq*-axis currents. The maximum torque per ampere (MTPA) control strategy has the advantages of minimizing copper losses and achieving maximum torque output with minimum current. Therefore, in the IPMSM control system, the MTPA control strategy can not only make full use of the reluctance torque, but also improve the torque output capability and the motor drive system efficiency [7], [8].

The main control methods of MTPA are as follows: the first method is the formula method. With this method, the torque equation is generally derived, and the relationship between the *dq*-axis currents and the torque is obtained from the derivative zero. For example, in reference [9], the relationship between the *dq*-axis currents and the torque is obtained by Lagrange iteration method, and the relationship curve between the *dq*-axis currents and torque is approximated linearized. In [10], the complexity of the MTPA control method is simplified, and an MTPA control method using integrated current vector equivalent replacement torque control is proposed. In addition, Shinohara *et al.* [11]–[13] considered the variation of inductance, the magnetic saturation and cross-coupling effect of PMSM, and proposed a flux linkage calculation method based on MTPA control.

The second method is the look-up table method. With this method, the inductance data is measured in advance by finite element software or static test. Then according to the relationship between the current and the torque, the corresponding *dq*-axis currents values under different torque are obtained,

The associate editor coordinating the review of this manuscript and approving it for publication was Yangmin Li.

and it is made into two-dimensional data table. For example, in [14], [15], the motor parameters are obtained by off-line experiments. Combined with the MTPA curve, current limit circle, MTPV curve, voltage limit and torque curve, the *dq*-axis currents data table is obtained by recursive method. During the control, the parameters are corrected according to the current value in a look-up table, and then the given values are calculated according to the modified parameters. In [16], considering the influence of temperature on MTPA control, an improved MTPA control current data table is obtained by the interpolation method based on the relation of temperature and torque. In reference [17], a table look-up method MTPA control without motor parameters is proposed, in this method, the demagnetization current is used as the reference by per unit normalization, and a general standardized torque-current data table is established.

The third method is the curve fitting method. With this method, Substituting the motor parameters or a given torque into the solution of the MTPA, the current or flux linkage reference value is calculated, and then the relationship between the given value and the torque or an observable variable is obtained by curve fitting, and finally the given value in real time is calculated by fitting the function relation. The main forms of fitting are as follows: the function of the *dq*-axis currents with the torque and flux linkage [18], [19], a function of the optimal torque angle and the stator current based on the MTPA control [20], [21], In addition, the MTPA control can be achieved by adopting a multi-segment curve fitting method, so that the fitting precision and the operation speed of the system can be improved [22], [23].

The fourth method is the auxiliary signal injection method. With this method, a known auxiliary signal is injected into a reference signal, then, the feedback signal and the injected signal are multiplied through the same high-pass filter, and later the low-pass filtering is performed. There are many injection methods, such as the current injection method, which superimposes the pulse current space vector on the steady-state component of the current, generates a certain torque under the steady state of speed and torque [24], [25], or calculates the MTPA angle by measuring the resulting rotational speed harmonic by the current injection motor [26]. Another method is the voltage vector injection, which directly injects the high-frequency signal into the voltage vector without considering the bandwidth of the speed loop and the current loop, and it does not need to modulate the signal, so it is easy to implement [27], [28]. Besides, so as to reduce the torque fluctuation and resonance problem, the current vector angle injection method is used to replace the actual signal of the injected current by injecting the virtual signal of the current angle [29].

In summary, the auxiliary signal injection method has strong robustness, and can better deal with the influence of the motor parameters change; however, its convergence speed is slow, and the injection of external signals can also cause different degrees of torque fluctuation, at the same time, high-frequency signal injection can also prone to harmonics resulting in increased losses. Compared with this, the curve fitting method is simple and easy to use, the calculation amount is small, and the accuracy can be improved by piecewise fitting; however, its robustness is poor. Although the look-up table method reduces the amount of calculation to a certain extent, the real-time performance is good and the accuracy is high; but it increases the workload of off-line testing, and a large amount of experimental calibration or fitting work is required, which increases the workload of the researcher, besides, it takes up a lot of storage space and the robustness is poor. The formula method is relatively compromised in terms of performance, and the robustness can be improved by using the method of online parameter identification, which is more practical. Therefore, in this paper, the formula method is used to realize the MTPA control of the system.

The control of the electric vehicle IPMSM is actually the control of the vehicle velocity during the driving process of the electric vehicle [30], but the existing motor control does not combine the driving state of the electric vehicle, and the impact of driving system control strategies on the electric vehicle energy consumption has not been considered. Therefore, the relationship between the electric vehicle driving state and the motor control is considered in this paper. On this basis, the MTPA control strategy of IPMSM (IPMSM-MTPA control strategy) based on the optimization acceleration curve is proposed, and the energy consumption of different acceleration curves are analyzed by simulation and experiment.

II. MATHEMATICAL MODELS OF IPMSM AND ELECTRIC VEHICLE ENERGY CONSUMPTION

A. IPMSM MATHEMATICAL MODEL

In the synchronous rotating coordinate system (*dq*-axis), according to the IPMSM coordinate transformation, the *dq*-axis stator voltages u_d and u_q can be calculated as follows:

$$\begin{cases} u_d = R_s i_d + \dfrac{d}{dt}\psi_d - \omega_e \psi_q \\ u_q = R_s i_q + \dfrac{d}{dt}\psi_q + \omega_e \psi_d \end{cases} \tag{1}$$

And the *dq*-axis stator flux linkages ψ_d and ψ_q can be expressed as the following equations:

$$\begin{cases} \psi_d = L_d i_d + \psi_f \\ \psi_q = L_q i_q \end{cases} \tag{2}$$

Substitution (2) into (1), the *dq*-axis stator voltages u_d and u_q can also be described by the following expression:

$$\begin{cases} u_d = R_s i_d + L_d \dfrac{d}{dt} i_d - \omega_e L_q i_q \\ u_q = R_s i_q + L_q \dfrac{d}{dt} i_q + \omega_e \left(L_d i_d + \psi_f \right) \end{cases} \tag{3}$$

The mechanical equation can be described as follows:

$$J \frac{d}{dt}\omega_m = T_e - T_m - B\omega_m \tag{4}$$

And the electromagnetic torque equation can be expressed as:

$$T_e = \frac{3}{2} p_n \left[\psi_f i_q + \left(L_d - L_q \right) i_q i_d \right] \tag{5}$$

where: u_d (V) and u_q (V) are the dq-axis stator voltages; i_d (A) and i_q (A) are the dq-axis stator currents; R_s (Ω) is the stator resistance; ψ_d (Wb) and ψ_q (Wb) are the dq-axis stator flux linkages; L_d (H) and L_q (H) are the dq-axis inductances; ψ_f (Wb) is the permanent magnet flux linkage; ω_e (rad/s) is the electrical angular speed, ω_m (rad/s) is the mechanical angular speed of the motor, and $\omega_m = \omega_e / p_n$; p_n is the number of pole pairs of the motor; J $(kg \cdot m^2)$ is the moment of inertia of the motor and load; B $(N \cdot s/m)$ is the damping coefficient; T_m $(N \cdot m)$ is the load torque of the motor; T_e $(N \cdot m)$ is the electromagnetic torque.

B. ELECTRIC VEHICLE ENERGY CONSUMPTION MODEL

On the basis of automobile theory [31], when the electric vehicle accelerates on good road, the slope of which can be neglected, the traction force $F_t(t)$ (N) can be calculated as follows:

$$F_t(t) = mgf + \frac{C_D A u(t)^2}{21.15} + \delta m a(t) \tag{6}$$

where m (kg) is the electric vehicle mass; f is the rolling friction coefficient; C_D is the drag coefficient; A (m^2) is the electric vehicle frontal area; δ is the electric vehicle rotating mass conversion factor; $u(t)$ (km/h) is the electric vehicle velocity; $a(t)$ (m/s^2) is the acceleration.

According to (6), the output power of the battery $P_b(t)$ (w) during the acceleration process can be expressed as:

$$P_b(t) = u(t) \cdot \left[mgf + \frac{C_D A u(t)^2}{21.15} + \delta m a(t) \right] \Big/ 3.6 \eta_T \eta_V \eta_m \tag{7}$$

where η_T is the efficiency of the transmission system; η_V is the efficiency of the inverter; η_m is the efficiency of the electric motor,

According to (7), the electric vehicle energy consumption per kilometer $E_{b-j}(t)$ (Wh/km) in an acceleration process is given as follows:

$$E_{b-j}(t) = \frac{\int_{t_0}^{t_f} u(t) \cdot \left[mgf + \frac{C_D A u(t)^2}{21.15} + \delta m a(t) \right] \Big/ 3.6 \eta_T \eta_V \eta_m dt}{\int_{t_0}^{t_f} u(t)\, dt} \tag{8}$$

According to (8), it can be found that, when the working conditions and road load are certain, m, f, C_D, A, δ can be regarded as constant values, $E_{b-j}(t)$ mainly depends on $u(t)$ and $a(t)$, $u(t)$ and $a(t)$ mainly depend on acceleration curves. Consequently, it is important that study different acceleration curves.

III. RELATIONSHIP BETWEEN MTPA CONTROL AND DRIVING STATE OF ELECTRIC VEHICLES

A. RELATIONSHIP BETWEEN DRIVING STATE OF ELECTRIC VEHICLE AND DQ-AXIS CURRENTS

The relationship between the load torque $T_m(t)$ $(N \cdot m)$ of the drive motor and the traction force $F_t(t)$ (N) can be expressed in the following way:

$$T_m(t) = \frac{F_t(t) r}{i_g i_o \eta_T} \tag{9}$$

And the relationship between the electric vehicle velocity $u(t)$ (km/h) and the drive motor speed $n_m(t)$ (r/min) can be expressed as:

$$u(t) = 0.377 \frac{r n_m(t)}{i_g i_o} \tag{10}$$

where i_g, i_o is the ratio of transmission and the ratio of the reducer, respectively; r (m) is the wheel radius.

Besides, the relationship between the drive motor speed $n_m(t)$ (r/min) and mechanical angular speed $\omega_m(t)$ (rad/s) can be expressed as:

$$\omega_m(t) = \frac{\pi n_m(t)}{30} \tag{11}$$

Therefore, according to (10) and (11), the relationship between the electric vehicle velocity $u(t)$ (km/h) and mechanical angular speed $\omega_m(t)$ (rad/s) can be described as:

$$u(t) = \frac{3.6 \omega_m(t)\, r}{i_g i_o} \tag{12}$$

In order to analyze the relationship between the driving state of the electric vehicle and dq-axis currents, the mechanical Equation (4) can be rewritten as:

$$T_e(t) = J \frac{d}{dt} \omega_m(t) + T_m(t) + B \omega_m(t) \tag{13}$$

According to (6), (12) and (13), the relationship between the electric vehicle velocity $u(t)$ (km/h), acceleration $a(t)$ (m/s^2) and electromagnetic torque $T_e(t)$ $(N \cdot m)$ can be described by the following expression:

$$T_e(t) = J \frac{d}{dt} \frac{u(t) i_g i_o}{3.6r} + \frac{mgfr + \frac{C_D A u(t)^2 r}{21.15} + \delta m a(t) r}{i_g i_o \eta_T} + B \frac{u(t) i_g i_o}{3.6r} \tag{14}$$

The above formula is organized and simplified as the following function:

$$T_e(t) = a_1 u(t)^2 + b_1 u(t) + c_1 a(t) + d_1 \tag{15}$$

where: $a_1 = C_D A r / (21.15 i_g i_o \eta_T)$, $b_1 = B i_g i_o / (3.6r)$, $c_1 = J i_g i_o / (3.6r) + \delta m r / (i_g i_o \eta_T)$, $d_1 = mgfr / (i_g i_o \eta_T)$.

According to (5) and (15), the relationship between the electric vehicle velocity $u(t)$ (km/h), acceleration $a(t)$ (m/s^2) and dq-axis currents can be obtained as follows:

$$a_1 u(t)^2 + b_1 u(t) + c_1 a(t) + d_1 = \frac{3}{2} p_n \left[\psi_f i_q + \left(L_d - L_q \right) i_q i_d \right] \tag{16}$$

The above analysis combines the relationship between the electric vehicle velocity and acceleration and the PMSM load torque, electromagnetic torque, and *dq*-axis currents, that is, the electric vehicle driving state is combined with the motor driving state, where the vehicle velocity and acceleration depend on the electric vehicle acceleration curve and the acceleration depends on the change in the vehicle velocity. When the electric vehicle accelerating, the driver can make the electric vehicle reach a certain desired velocity by operating the accelerator pedal. Therefore, the vehicle velocity can be used as the motor drive system control goal, and the electric vehicle can be controlled to drive according to a given acceleration curve by controlling the *dq*-axis currents (i_d and i_q).

B. MAXIMUM TORQUE PER AMPERE (MTPA) METHOD

MTPA control is a common current control strategy for IPMSM. For IPMSM, its electromagnetic torque is divided into reluctance torque and permanent magnet torque. Due to the asymmetrical structure of the rotor magnetic circuit, the *dq*-axis inductances are not equal (generally: $L_\mathrm{d} < L_\mathrm{q}$), and thus have reluctance torque. If the value of i_d is controlled reasonably, the reluctance torque can be used to increase the power density and overload capability of the motor. To this end, the goal of using the MTPA control strategy is to make full use of the motor reluctance torque, so that the unit current can output maximum torque, thereby improving the motor system efficiency.

The MTPA control designs the control strategy from electromagnetic torque and motor stator current, with the maximum ratio of torque to current as the target. Compared with $i_d = 0$ control, this control strategy increases the control of the *q*-axis current, by modulating the amplitude and angle of the motor stator current vector, the ratio of the output electromagnetic torque to the stator current is kept to the maximum. And in the case of outputting the same electromagnetic torque, the stator current consumed by MTPA is smaller, the copper consumption is smaller and the system efficiency is higher. Therefore, the MTPA control strategy is more suitable for the IPMSM of the electric vehicle.

In this paper, the formula method is used for online real-time control. The MTPA control of the formula method is essentially to find the extreme point of the *dq*-axis currents, that is, the optimization problem of the stator current i_s under the electromagnetic torque condition, namely:

$$\begin{cases} \min \quad i_\mathrm{s} = \sqrt{i_\mathrm{d}^2 + i_\mathrm{q}^2} \\ \text{s.t.} \quad T_\mathrm{e} = \dfrac{3P_\mathrm{n}}{2}\left[\psi_\mathrm{f} i_\mathrm{q} + \left(L_\mathrm{d} - L_\mathrm{q}\right) i_\mathrm{d} i_\mathrm{q}\right] \end{cases} \tag{17}$$

The optimization solution of MTPA control algorithm can be solved by Lagrange multiplier method, and the extreme value of the functions with multiple variables and constraint conditions can be solved by constructing Lagrange auxiliary functions. The Lagrange auxiliary function for Equation (17) is given as follows:

$$F = \sqrt{i_\mathrm{d}^2 + i_\mathrm{q}^2} + \lambda\left\{T_\mathrm{e} - \frac{3P_\mathrm{n}}{2}\left[\psi_\mathrm{f} i_\mathrm{q} + \left(L_\mathrm{d} - L_\mathrm{q}\right) i_\mathrm{d} i_\mathrm{q}\right]\right\} \tag{18}$$

where: λ is the Lagrange multiplier. Let (18) be partial derivation to λ, i_d and i_q, respectively, and let the derivative be zero, the following formula can be obtained:

$$\begin{cases} \dfrac{\partial F}{\partial \lambda} = T_\mathrm{e} - \dfrac{3}{2}P_\mathrm{n}\left[\psi_\mathrm{f} i_\mathrm{q} + \left(L_\mathrm{d} - L_\mathrm{q}\right) i_\mathrm{d} i_\mathrm{q}\right] = 0 \\ \dfrac{\partial F}{\partial i_\mathrm{d}} = \dfrac{i_\mathrm{d}}{\sqrt{i_\mathrm{d}^2 + i_\mathrm{q}^2}} - \dfrac{3}{2}\lambda P_\mathrm{n}\left(L_\mathrm{d} - L_\mathrm{q}\right) i_\mathrm{q} = 0 \\ \dfrac{\partial F}{\partial i_\mathrm{q}} = \dfrac{i_\mathrm{q}}{\sqrt{i_\mathrm{d}^2 + i_\mathrm{q}^2}} - \dfrac{3}{2}\lambda P_\mathrm{n}\left[\psi_\mathrm{f} + \left(L_\mathrm{d} - L_\mathrm{q}\right) i_\mathrm{d}\right] = 0 \end{cases} \tag{19}$$

According to (19), the relationship between i_d and i_q is derived as follows:

$$\begin{cases} i_d = \dfrac{-\psi_f \pm \sqrt{\psi_f^2 + 4i_q^2\left(L_d - L_q\right)^2}}{2\left(L_d - L_q\right)} \\ i_\mathrm{q} = \sqrt{\dfrac{\psi_\mathrm{f} i_\mathrm{d}}{L_\mathrm{d} - L_\mathrm{q}} + i_d^2} \end{cases} \tag{20}$$

Because in MTPA control, $i_\mathrm{d} < 0$ and $L_d < L_q$, then the above formula can be expressed as:

$$\begin{cases} i_d = \dfrac{-\psi_f + \sqrt{\psi_f^2 + 4i_q^2\left(L_d - L_q\right)^2}}{2\left(L_d - L_q\right)} \\ i_\mathrm{q} = \sqrt{\dfrac{\psi_\mathrm{f} i_\mathrm{d}}{L_\mathrm{d} - L_\mathrm{q}} + i_d^2} \end{cases} \tag{21}$$

By substituting any one of the (21) into the electromagnetic torque (5), the relationship between the*dq*-axis currents and the electromagnetic torque (i.e., $i_d = f_1(T_e)$ and $i_q = f_2(T_e)$) can be obtained. However, $i_d = f_1(T_e)$ and $i_q = f_2(T_e)$ are higher-order equation, it is difficult to implement in engineering. In order to simplify the complexity of the control, the control of the torque (T_e) can be equivalent to the control of the stator current vector (i_s) by the relationship between the torque and the current. Therefore, according to (17) and (21), the relationship between the *dq*-axis currents i_d, i_q and the stator current i_s can be obtained as follows:

$$\begin{cases} i_d = \dfrac{-\psi_f \pm \sqrt{\psi_f^2 + 8i_s^2\left(L_d - L_q\right)^2}}{4\left(L_d - L_q\right)} \\ i_q = \sqrt{i_s^2 - i_d^2} \end{cases} \tag{22}$$

Similarly, due to in MTPA control, $i_\mathrm{d} < 0$ and $L_d < L_q$, then the (22) can be expressed as:

$$\begin{cases} i_d = \dfrac{-\psi_f + \sqrt{\psi_f^2 + 8i_s^2\left(L_d - L_q\right)^2}}{4\left(L_d - L_q\right)} \\ i_q = \sqrt{i_s^2 - i_d^2} \end{cases} \tag{23}$$

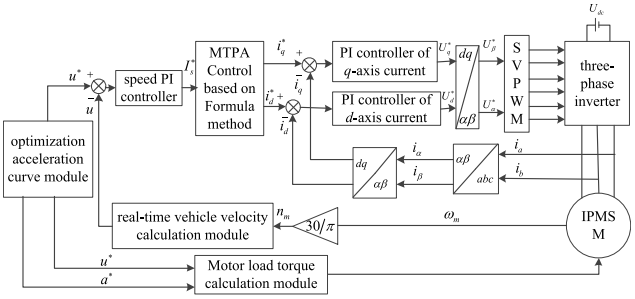

FIGURE 1. The IPMSM-MTPA control block diagram based on optimization acceleration curve.

Equation (23) is the optimal i_d, i_q for the MTPA control, combined with (16), by controlling different i_d and i_q, the electric vehicle can be driven according to different acceleration curves. When the IPMSM adopts the MTPA control, the IPMSM loss can be reduced, the electric vehicle energy consumption per kilometer can also be reduced, so as to the driving range will be increased.

IV. MTPA CONTROL AND SIMULATION ANALYSIS OF IPMSM BASED ON OPTIMIZATION ACCELERATION CURVE

A. MTPA CONTROL OF IPMSM BASED ON OPTIMIZATION ACCELERATION CURVE

According to the optimization acceleration curve of electric vehicle, the vehicle controller sends a vehicle velocity command to the driving motor controller, and the driving motor controller controls the output torque of the driving motor to drive the electric vehicle forward according to its loaded control strategy. Therefore, in this paper, based on the optimization acceleration curve of electric vehicle, an IPMSM-MTPA control strategy for electric vehicle is established. And the control block diagram is shown in Fig. 1.

As shown in Fig. 1, the control principle of the proposed control strategy is: first, the vehicle velocity u^* in the optimization acceleration curve (u^* and a^*) module [32] is used as the target vehicle velocity; then, the difference between the target vehicle velocity u^* and the current real-time vehicle velocity u is transmitted to the MTPA control module as the reference stator current I_s^* via the speed PI controller; the MTPA control module calculates the optimal dq-axis reference currents i_d^* and i_q^* according to the corresponding formula; and the difference between the dq-axis feedback currents i_d and i_q and the dq-axis reference currents i_d^* and i_q^* is modulated by the PI controller to obtain the reference dq-axis voltages U_d^* and U_q^*; Then, after anti-park transformation, the reference voltages U_α^* and U_β^* under $\alpha\beta$ coordinates are obtained, and the U_α^* and U_β^* voltages signals are modulated by SVPWM and output PWM signals to the three-phase inverter, the three-phase inverter is controlled to output three-phase currents i_a, i_b and i_c, and the three-phase currents drives the PMSM to make the vehicle drive at a given vehicle velocity. At the same time, the real-time vehicle velocity calculation module calculates the current vehicle velocity feedback value u according to the current motor speed n_m; The three-phase currents, i_a, i_b and i_c are clark transformed to obtain the $\alpha\beta$-axis currents i_α and i_β, the i_α and i_β are park transformed to obtain dq-axis currents i_d and i_q, and compared with the given dq-axis currents i_d^* and i_q^*. The control system is carried out repeatedly as described above, so that the vehicle runs according to the given acceleration curve.

TABLE 1. The parameters of NEDC urban conditions and optimization acceleration curves.

Velocity (km/h)	Acceleration condition	Acceleration time t_i /(s)	Acceleration a_i /(m/s^2)
0-32	Optimization acceleration curve	$t_1^* = 3.88$	$a_1^* = 1.2$
		$t_2^* = 6.12$	$a_2^* = 0.69$
	NEDC	$t_1 = 5$	$a_1 = 0.83$
		$t_2 = 5$	$a_2 = 0.94$
0-50	Optimization acceleration curve	$t_1^* = 4.2$	$a_1^* = 1.2$
		$t_2^* = 6.0$	$a_2^* = 0.8$
		$t_3^* = 4.6$	$a_3^* = 0.6$
		$t_4^* = 7.2$	$a_4^* = 0.18$
	NEDC	$t_1 = 5$	$a_1 = 0.83$
		$t_2 = 9$	$a_2 = 0.61$
		$t_3 = 8$	$a_3 = 0.52$
0-70	Optimization acceleration curve	$t_1^* = 5.4$	$a_1^* = 1.2$
		$t_2^* = 4.6$	$a_2^* = 0.9$
		$t_3^* = 7.8$	$a_3^* = 0.7$
		$t_4^* = 10$	$a_4^* = 0.22$
		$t_5^* = 7.2$	$a_5^* = 0.17$
	NEDC	$t_1 = 5$	$a_1 = 0.83$
		$t_2 = 9$	$a_2 = 0.61$
		$t_3 = 8$	$a_3 = 0.52$
		$t_4 = 13$	$a_4 = 0.43$

And in Fig. 1, the acceleration curve in the optimization acceleration curve module [32] is optimized by the fast elitist non-dominated sorting genetic (NSGA-II) algorithm. In this work, both energy consumption and battery life are simultaneously considered, the total acceleration time is constant for a given velocity, the acceleration values and acceleration time are used as the decision variable, and the energy consumption and the battery capacity loss are taken as the optimization objectives. And the optimization results are shown in Table 1.

Among them, the PI control is used in speed and dq-axis currents controller. The PI control takes the error between the output value and the expected value of the system as the input signal, and the proportional and the integral of the error signal are linearly combined to solve the required controlled variable of the control system. The PI control principle can be expressed by the following formula:

$$u(t) = K_P e(t) + K_I \int e(t)\, dt \tag{24}$$

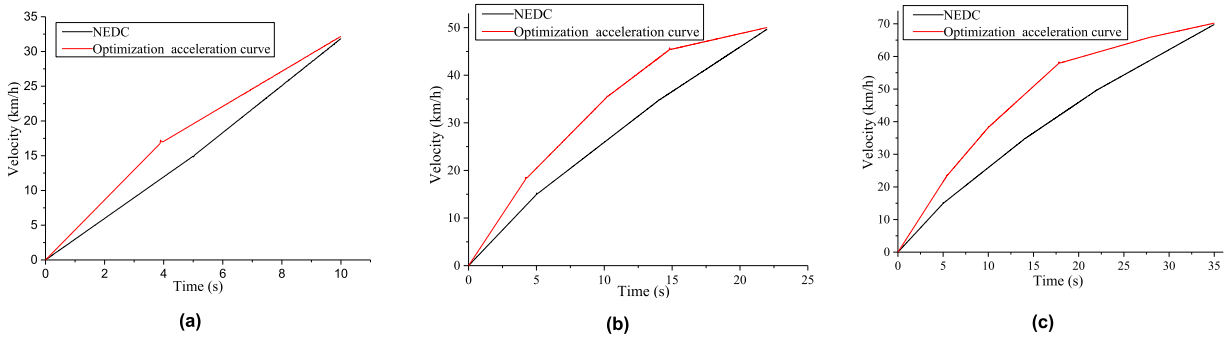

FIGURE 2. The electric vehicle velocity simulation results of NEDC and optimization acceleration curve. (a) Vehicle velocity change of 0-32km/h. (b) Vehicle velocity change of 0-50km/h. (c) Vehicle velocity change of 0-70km/h.

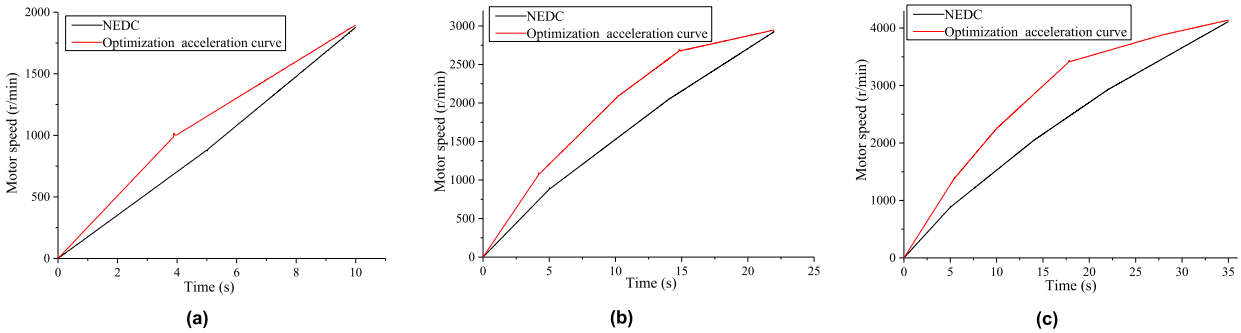

FIGURE 3. The motor speed simulation results of NEDC and optimization acceleration curve. (a) Motor speed change 0-32km/h. (b) Motor speed change 0-50km/h. (c) Motor speed change 0-70km/h.

where: K_P, K_I are proportional and integral coefficients; $e(t)$ is the error between the output value and the expected value of the system. The K_P and K_I coefficients reflect their proportion in the control system, and finding the optimal combination of K_P and K_I is the key to PI control. The common parameter setting methods of PI control are formula method, trial and error method, empirical method and so on.

B. SIMULATION RESULTS AND ANALYSIS

In order to verify the effectiveness of PMSM-MTPA control strategy of the electric vehicle based on the optimization acceleration curve, the corresponding simulation model is established based on Matlab/Simulink simulation software, and the simulation and analysis are carried out.

Due to the motor bench experimental platform built later in this paper is limited by the rated power and rated torque of the drive motor, and combined with the electric vehicle theory, the maximum vehicle mass that can be simulated by the motor bench is 500kg, and the maximum vehicle velocity that can be simulated is about 70km/h. Therefore, in order to ensure the safety of the experiment and compare the simulation with the experiment, in this paper, the load torque of the drive motor is calculated according to the electric vehicle curb weight of 300kg. And the motor stator resistance R_s is 0.05 Ω, the d-axis inductance L_d is 0.000174H, the q-axis inductance L_q is 0.000293H, the permanent magnet flux linkage ψ_f is 0.0711Wb, the moment of inertia J is 0.003 $kg \cdot m^2$, the damping coefficient B is 0.0008 $N \cdot s/m$.

Therefore, in this paper, the acceleration conditions (0-32km/h, 0-50km/h and 0-70km/h) in NEDC urban conditions are selected to analyze, and the NEDC urban conditions and the corresponding optimization acceleration curves are simulated and analyzed respectively. The working condition characteristic parameters of NEDC urban conditions and corresponding optimization acceleration curves [32] are shown in Table 1.

The simulation results of the electric vehicle velocity and the motor speed of the NEDC urban conditions and the corresponding optimization acceleration curves are shown in Fig. 2-3. And the simulation results of the driving range, the electric energy consumption, and energy consumption per kilometer of the NEDC urban conditions and the optimization acceleration curves are shown in Table 2.

From Fig. 2, it can be seen that, the optimization acceleration curves are all above the NEDC urban conditions, and the accelerations of the optimization acceleration curves are all getting smaller and smaller. From Fig.3, it can be found that, according to the relationship between the electric vehicle velocity and the motor speed (refer to (10)), the change trend of the motor speed is consistent with the vehicle velocity. In addition, from the simulation results in Table 2, it can be found that for 0-32km/h, compared with the NEDC urban condition, the driving range of the optimization acceleration curve increases by 17.95%, and the energy consumption per kilometer reduces by 10.69%. For 0-50km/h, compared with the NEDC urban condition, the driving range of optimization

TABLE 2. Statistics on simulation results of different acceleration curves.

Velocity(km/h)	Acceleration condition	Driving range （km）	Electric energy consumption （Wh）	Energy consumption per kilometer E_{b-j} （Wh/km）
0-32	NEDC	0.0429	4.7504	110.8037
	Optimization acceleration curve	0.0506	5.0110	98.9548
0-50	NEDC	0.1662	13.7422	82.6899
	Optimization acceleration curve	0.2022	15.6983	77.6266
0-70	NEDC	0.3819	34.0683	89.2019
	Optimization acceleration curve	0.4688	41.7999	89.1671

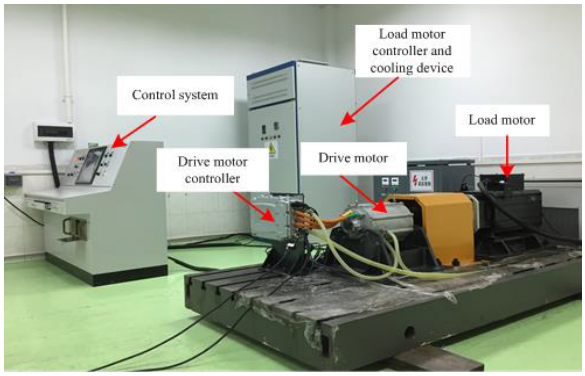

FIGURE 4. The electric vehicle drive system control experimental platform physical.

acceleration curve increases by 21.66%, and the energy consumption per kilometer reduces by 6.12%. And for 0-70km/h, compared with the NEDC urban condition, the driving range of optimization acceleration curve increases by 22.75%, and the energy consumption per kilometer reduces by 0.04%.

V. EXPERIMENTAL VERIFICATIONS

In order to verify the feasibility and effectiveness of different acceleration control strategies, the motor bench experiments for the electric vehicle are established, and the motor bench tests for different acceleration control strategies are carried out.

The motor bench mainly includes: power battery, industrial control computer, motor controller, driving motor (PMSM), load motor, torque sensor, current and voltage sensor, data acquisition system and so on. The physical map is shown in Fig. 4. Which the inverter converts the direct current of the power battery into a suitable three-phase electricity to the drive motor, and the load motor is connected with the drive motor through a coupling and a torque sensor, so as to simulate the load torque in the electric vehicle driving process.

Before the experiment, according to the relationship between the electric vehicle acceleration curve and the motor speed and the motor torque, the relationship between the driving motor speed and the torque with time is input into the control system. During the experiment, the control system transmits the motor speed command to the motor controller, which drives the motor to run according to the given speed.

TABLE 3. Main parameters of the PMSM.

Parameters	Value
Motor rated power （kW）	25
Motor rated torque （ $N \cdot m$ ）	133
Motor rated speed （r/min）	1800
Motor peak power （kW）	56kW
Motor peak torque （ $N \cdot m$ ）	350Nm
Motor peak speed （r/min）	4000

And in order to simulate the load torque when the electric vehicle accelerates, the load motor controller makes the load motor output a corresponding torque according to the load command. At the same time, the data acquisition card will collect the power battery voltage, current and torque signals, and the CAN communication card will collect the motor speed signals, and transmit these signals to the control system for storage.

The parameters of the PMSM used in the experiment are shown in Table 3.

Based on the relationship between the electric vehicle velocity and the motor speed, the electric vehicle velocity can be obtained. Fig. 5-7 shows the experimental results of the vehicle velocity, the motor torque and the battery output power of NEDC urban conditions and corresponding optimization acceleration curves. And Table 4 shows the motor bench experimental results for the driving range, electric energy consumption and energy consumption per kilometer of different acceleration curves.

From Fig. 5, it can be found that, the experimental results of electric vehicle velocity are consistent with the simulation results. Since the change trend of the motor speed is the same as the vehicle velocity, the experimental results of the motor speed here are not listed. From Fig. 6, it can be seen that the torque is related to the acceleration, the larger the acceleration is, and the larger the torque is. And from Fig. 7, it can be also found that, the battery output power is also related to the acceleration, the larger the acceleration is, the larger the current is, and the larger the battery output power is. Besides, from the motor bench experimental results in Table 4, it can be found that for 0-32km/h, compared with the NEDC urban condition, the driving range of the optimization acceleration curve increases by 17.12%, and the energy consumption per kilometer reduces by 10.44%. For 0-50km/h, compared with

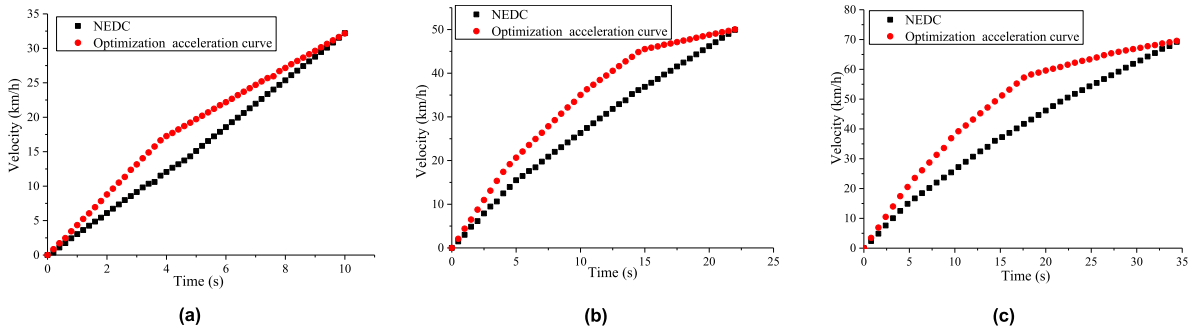

FIGURE 5. The electric vehicle velocity experimental results of NEDC and optimization acceleration curve. (a) Vehicle velocity change of 0-32km/h. (b) Vehicle velocity change of 0-50km/h. (c) Vehicle velocity change of 0-70km/h.

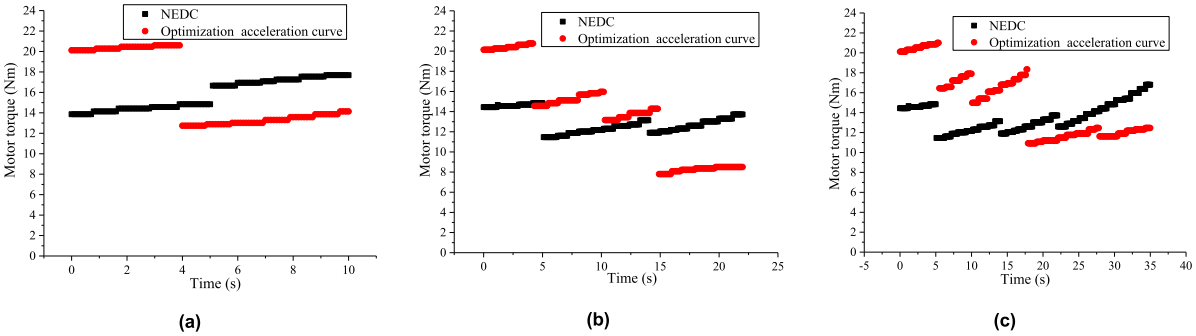

FIGURE 6. The motor torque experimental results of NEDC and optimization acceleration curve. (a) Motor torque change of 0-32km/h. (b) Motor torque change of 0-50km/h. (c) Motor torque change of 0-70km/h.

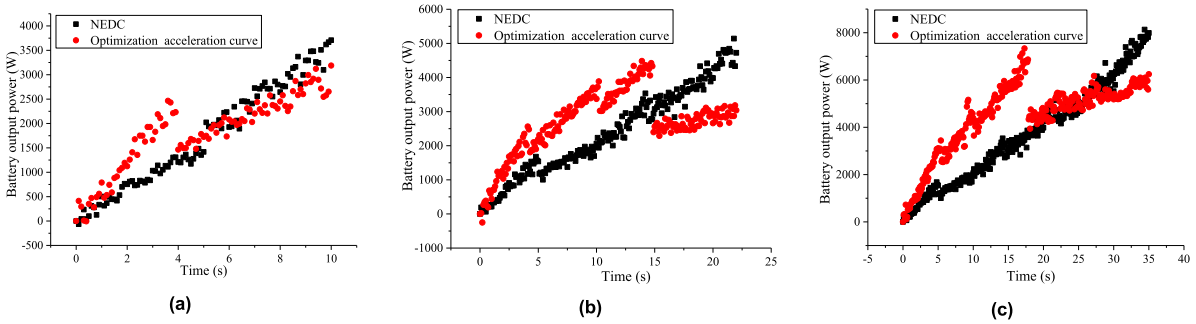

FIGURE 7. The battery output power experimental results of NEDC and optimization acceleration curve. (a) Battery output power change of 0-32km/h. (b) Battery output power change of 0-50km/h. (c) Battery output power change of 0-70km/h.

TABLE 4. Statistics on the motor bench experimental results of different acceleration curves.

Velocity(km/h)	Acceleration conditions	Driving range （km）	Electric energy consumption （Wh）	Energy consumption per kilometer E_{b-j} （Wh/km）
0-32	NEDC	0.0438	4.8608	110.9816
	Optimization acceleration curve	0.0513	5.0950	99.3905
0-50	NEDC	0.1689	14.5428	86.1056
	Optimization acceleration curve	0.2035	16.4671	80.9044
0-70	NEDC	0.3859	36.0392	93.3880
	Optimization acceleration curve	0.4687	43.4251	92.6550

the NEDC urban condition, the driving range of optimization acceleration curve increases by 20.49%, and the energy consumption per kilometer reduces by 6.04%. And for 0-70km/h, compared with the NEDC urban condition, the driving range of optimization acceleration curve increases by 21.46%, and the energy consumption per kilometer reduces by 0.78%.

From the above analysis, it can be found that the experimental results and the simulation results are consistent with

the previous research results [32], that is, when the electric vehicle accelerates with the optimization acceleration curves, its energy consumption per kilometer is less than NEDC urban conditions, and its driving range is longer than NEDC urban conditions. The analysis above also verifies the validity of the proposed control strategy in this paper.

VI. CONCLUSION

In view of the problem that the existing motor drive system control technology does not consider the energy consumption of electric vehicles, the relationship between the electric vehicle driving state and electromagnetic torque, MTPA *dq*-axis currents is analyzed. On this basis, the IPMSM-MTPA control strategy based on the optimization acceleration curve is proposed, and the simulation was carried out by Matlab/Simulink software. In order to further verify the feasibility and effectiveness of different acceleration control strategies, the corresponding motor test benches is built, and the motor bench experiments with different acceleration curves are carried out. The simulation and experimental results show that compared with the NEDC urban conditions, the driving range of the electric vehicle drive system control strategy based on the optimization acceleration curve is improved, and the energy consumption per kilometer of the electric vehicle is reduced, which verifies the proposed drive system control strategy.

REFERENCES

[1] J. Lara, J. Xu, and A. Chandra, "Effects of rotor position error in the performance of field oriented controlled PMSM drives for electric vehicle traction applications," *IEEE Trans. Ind. Electron*, vol. 63, no. 8, pp. 4738–4751, Aug. 2016.

[2] X. Zhang, D. Göhlich, and J. Li, "Energy-efficient toque allocation design of traction and regenerative braking for distributed drive electric vehicles," *IEEE Trans. Veh. Technol.*, vol. 67, no. 1, pp. 285–295, Jan. 2018.

[3] C. Zhang, S. Zhang, G. Han, and H. Liu, "Power management comparison for a dual-motor-propulsion system used in a battery electric bus," *IEEE Trans. Ind. Electron*, vol. 64, no. 5, pp. 3873–3882, May 2017.

[4] X. Liu, H. Chen, J. Zhao, and A. Belahcen, "Research on the performances and parameters of interior PMSM used for electric vehicles," *IEEE Trans. Ind. Electron.*, vol. 63, no. 6, pp. 3533–3545, Jun. 2016.

[5] Q. Liu and K. Hameyer, "High performance adaptive torque control for an IPMSM with real time MTPA operation," *IEEE Trans. Energy Convers.*, vol. 32, no. 2, pp. 571–581, Dec. 2016.

[6] C. Y. Wang, J. K. Xia, and Y. B. Sun, *Modern Motor Control Technology*. Beijing, China: China Machine Press, 2014.

[7] Y. Jeong, S. Sul, S. Hiti, and K. M. Rahman, "Online minimum-copper-loss control of an interior permanent-magnet synchronous machine for automotive applications," *IEEE Trans. Ind. Appl.*, vol. 42, no. 5, pp. 1222–1229, Sep. 2006.

[8] S. Bozhko, S. Dymko, S. Kovbasa, and S. M. Peresada, "Maximum torque-per-amp control for traction IM drives: Theory and experimental results," *IEEE Trans. Ind. Appl.*, vol. 53, no. 1, pp. 181–193, Sep. 2016.

[9] C. H. Li, M. J. Chen, and X. Y. Wu, "Study of a maximum ratio of torque to current control method for PMSM," *Proc. CSEE*, vol. 25, no. 21, pp. 169–174, Nov. 2005.

[10] S. K. Zhang, J. H. Yan, and K. Yang, "Interior permanent magnet synchronous motor control system for electric vehicle based on improved maximum torque per ampere method," *Electr. Mach. Control Appl.*, vol. 44, no. 11, pp. 16–21, Nov. 2017.

[11] A. Shinohara, Y. Inoue, S. Morimoto, and M. Sanada, "Direct calculation method of reference flux linkage for maximum torque per ampere control in DTC-based IPMSM drives," *IEEE Trans. Power Electron*, vol. 32, no. 3, pp. 2114–2122, May 2016.

[12] T. Inoue, Y. Inoue, S. Morimoto, and M. Sanada, "Maximum torque per ampere control of a direct torque controlled PMSM in a stator flux linkage synchronous frame," *IEEE Trans. Ind. Appl.*, vol. 52, no. 3, pp. 2360–2367, Feb. 2016.

[13] T. Inoue, Y. Inoue, S. Morimoto, and M. Sanada, "Mathematical model for MTPA control of permanent-magnet synchronous motor in stator flux linkage synchronous frame," *IEEE Trans. Ind. Appl.*, vol. 51, no. 5, pp. 3620–3628, Mar. 2015.

[14] B. Cheng and T. R. Tesch, "Torque feedforward control technique for permanent-magnet synchronous motors," *IEEE Trans. Ind. Electron.*, vol. 57, no. 3, pp. 969–974, Mar. 2010.

[15] H. Ge, Y. Miao, B. Bilgin, B. Nahid-Mobarakeh, and A. Emadi, "Speed range extended maximum torque per ampere control for PM drives considering inverter and motor nonlinearities," *IEEE Trans. Power Electron*, vol. 32, no. 9, pp. 7151–7159, Nov. 2017.

[16] Y. S. Kim and S. K. Sul, "Torque control strategy of an IPMSM considering the flux variation of the permanent magnet," in *Proc. IEEE Ind. Appl. Annu. Meeting*, Sep. 2007, pp. 1301–1307.

[17] L. Hang and X. Y. Wang, "Universal maximum torque per ampere control for permanent magnet synchronous motor," *Micromotors*, vol. 49, no. 7, pp. 58–61, Jul. 2016.

[18] S. Huang, Z. Chen, K. Huang, and J. Gao, "Maximum torque per ampere and flux-weakening control for PMSM based on curve fitting," in *Proc. IEEE Vehicle Power Propuls. Conf.*, Sep. 2010, pp. 1–5.

[19] Y. Miao, H. Ge, M. Preindl, J. Yu, B. Cheng, and A. Emadi, "MTPA fitting and torque estimation technique based on a new flux-linkage model for interior-permanent-magnet synchronous machines," *IEEE Trans. Ind. Appl.*, vol. 53, no. 6, pp. 5451–5460, Jul. 2017.

[20] Y. Liao, Z. D. Wu, and R. Liu, "Improved maximum torque per ampere control strategy study for PMSM used in electric vehicles," *Electr. Mach. Control*, vol. 16, no. 1, pp. 12–17, Jan. 2012.

[21] X. X. Li and F. J. Deng, "Research of maximum torque per ampere control for permanent magnet synchronous motor," *Small Special Electr. Mach.*, vol. 44, no. 6, pp. 63–65 and 69, Jun. 2016.

[22] W. J. Zhang, Y. J. Feng, S. D. Huang, and J. Gao, "The maximum torque per ampere control of permanent magnet synchronous motor based on iterative method," *Trans. China Electrotechn. Soc.*, vol. 28, no. 2, pp. 402–407, 2013.

[23] J. Sun, X. Luo, and X. Ma, "Realization of maximum torque per ampere control for IPMSM based on inductance segmentation," *IEEE Access*, vol. 6, pp. 66088–66094, 2018.

[24] S. Bolognani, R. Petrella, A. Prearo, and L. Sgarbossa, "Automatic tracking of MTPA trajectory in IPM motor drives based on AC current injection," *IEEE Trans. Ind. Appl.*, vol. 47, no. 1, pp. 105–114, Nov. 2010.

[25] S. Kim, Y.-D. Yoon, S.-K. Sul, and K. Ide, "Maximum torque per ampere (MTPA) control of an IPM machine based on signal injection considering inductance saturation," *IEEE Trans. Power Electron.*, vol. 28, no. 1, pp. 488–497, Jan. 2013.

[26] C. Y. Lai, G. D. Feng, J. Tjong, and N. C. Kar, "Direct calculation of maximum-torque-per-ampere angle for interior PMSM control using measured speed harmonic," *IEEE Trans. Power Electron.*, vol. 33, no. 11, pp. 9744–9752, Jan. 2018.

[27] G. Liu, J. Wang, W. Zhao, and Q. Chen, "A novel MTPA control strategy for IPMSM drives by space vector signal injection," *IEEE Trans. Ind. Electron*, vol. 64, no. 12, pp. 9243–9252, Jun. 2017.

[28] S. Wang, K. Yang, and K. Chen, "An improved position-sensorless control method at low speed for PMSM based on high-frequency signal injection into a rotating reference frame," *IEEE Access*, vol. 7, pp. 86510–86521, 2019.

[29] T. Sun, J. Wang, and X. Chen, "Maximum torque per ampere (MTPA) control for interior permanent magnet synchronous machine drives based on virtual signal injection," *IEEE Trans. Power Electron.*, vol. 30, no. 9, pp. 5036–5045, Sep. 2015.

[30] X. H. Jiao and S. Li, "Adaptive speed tracking control of electric vehicles driven by permanent magnet synchronous motor," *Electr. Mach. Control*, vol. 15, no. 11, pp. 83–89, Nov. 2011.

[31] Z. S. Yu, *Automobile Theory*, 5th ed. Beijing, China: China Machine Press, 2009, pp. 3–18.

[32] L. F. Li and Q. Liu, "Acceleration curve optimization for electric vehicle based on energy consumption and battery life," *Energy*, vol. 163, no. 15, pp. 1039–1053, Feb. 2019.

LIFU LI received the M.S. degree in mechanical manufacture and automation and the Ph.D. degree in precision instrument from Chongqing University, Chongqing, China, in 1991 and 1996, respectively.

He is currently a Professor with the School of Mechanical and Automotive Engineering, South China University of Technology, Guangzhou, China. He has conducted more than 20 projects and has published more than 100 journal articles and conference proceedings. His research interests include electric vehicle design and control method, motor drive system control technology, intelligent connected vehicle technology, vehicle test technology and fault diagnosis, modern electromechanical measurement, and control technology.

QIN LIU received the B.S. degree in automobile service engineering and the M.S. degree in mechanical engineering from the Qilu University of Technology, Jinan, China, in 2014 and 2016, respectively. She is currently pursuing the Ph.D. degree in mechanical engineering with the South China University of Technology, Guangzhou, China.

Her research interests include electric vehicle design and control method, and motor drive system control technology.